

Understanding the nanoscale structure of hexagonal phase lyotropic liquid crystal membranes

Benjamin J. Coscia Douglas L. Gin Richard D. Noble Joe Yelk
Matthew Glaser Xunda Feng Michael R. Shirts

November 29, 2017

Introduction

Nanostructured membrane materials have become increasingly popular for aqueous separations applications such as desalination and biorefinement because they offer the ability to control membrane architecture at the atomic scale allowing the design of solute-specific separation membranes. [1]

- Most membrane-based aqueous separations of small molecules can be achieved using reverse osmosis (RO) or nanofiltration (NF) [2]

While RO and NF have seen many advances in the past few decades, they are far from perfect separation technologies.

- *RO membranes*

- Inconsistent performance : Current state-of-the-art RO membranes are unstructured with tortuous and polydisperse diffusion pathways which leads to inconsistent performance [3]
- High energy requirements : Necessarily high feed pressures drive up energy requirements which strains developing regions and contributes strongly to CO₂ emissions. [4]
- Separation based on differences in solubility and diffusivity: Moreover, designing RO membranes to achieve targeted separations of specific solutes is nearly impossible because various solutes dissolve into and diffuse through the polymer matrix at different rates. [5]

- At best, one can exploit these differences to create a functional selective barrier.

- *NF membranes*

- NF was introduced as an intermediate between RO and ultrafiltration, having the ability to separate organic matter and salts on the order of one nanometer in size.
- Larger and well-defined pores drive down energy requirements while still affording separation of solutes as small as ions to some degree [2]
- NF is often used as a precursor to reverse osmosis
- Unfortunately, NF membranes, like RO, possess a pore size distribution which limits their ability to perform precise separations [6]

Nanostructured membranes can bypass many of the performance issues which plague traditional NF and RO membranes.

- Tune size and functionality of building blocks to control pore size and shape: One can accomplish targeted separations with high selectivity by tuning shape, size and functionality of the molecular building blocks which form these materials.

- As a result, solute rejecting pores can have their sizes tuned uniformly, resulting in strict size cut-offs.
- Entirely different mechanisms may govern transport in a given nanostructured material which can inspire novel separation techniques.

Development of nanostructured materials has been limited by the ability to synthesize and scale various fundamentally sound technologies.

- Graphene sheets are atomically thick which results in excellent permeability but defects during manufacturing severely impact selectivity. [7]
- Molecular dynamics simulations of carbon nanotubes show promise [1] but synthetic techniques are unable to achieve scalable alignment and pore monodispersity.[8, 9]
- Zeolites have sub-nm pores with a narrow pore size distribution and MD simulations exhibit complete rejection of solvated ions, [10] however, experimental rejection was low and attributed to interstitial defects formed during membrane synthesis [11]
- There is a need for a scalable nanostructured membrane

Self assembling lyotropic liquid crystals (LLCs) are a suitable candidate for aqueous separation applications.

- LLCs share the characteristic ability of nanostructured membrane materials to create highly ordered structures with the added benefits of low cost and synthetic techniques feasible for large scale production [12]
- Neat liquid crystal monomer forms the thermotropic, Col_h phase. The presence of water results in the H_{II} phase.
- In both cases, monomers assemble into mesophases made of hexagonally packed, uniform size, cylinders with hydrophilic groups oriented inward towards the pore center and hydrophobic groups facing outward.
- H_{II} and Col_h phase systems created by the monomer named Na-GA3C11 have been extensively studied experimentally [13, 14, 15, 12, 16].
- Until recently, mesophases formed by Na-GA3C11 could not be macroscopically aligned, resulting in low flux membranes, slowing research in the field.
- In 2014, Feng et al. showed that the mesophases could be aligned using a magnetic field with subsequent crosslinking to lock the structure in place [12]
- In 2016, Feng et al. showed that the same result could be obtained using a technique termed soft confinement [16].
- Following this breakthrough, research into LLC membranes has been reinvigorated.

A molecular level understanding of LLC membrane structure, enabled by molecular dynamics simulations, will provide guidelines to reduce the large chemical space available to design monomers for creation of separation-specific membranes.

- Over the past 20 years, H_{II} phase LLC membrane studies have been limited primarily to Na-GA3C11 with some characterization done after minor structural modifications [17].
- Rejection studies show that this membrane can not perform separations of solutes less than 1.2 nm in diameter because the pores are too large [14].
- We do not yet understand how to reduce the effective pore size or how to tune the chemical environment in the nanopores for effective water desalination or small organic molecule separations.

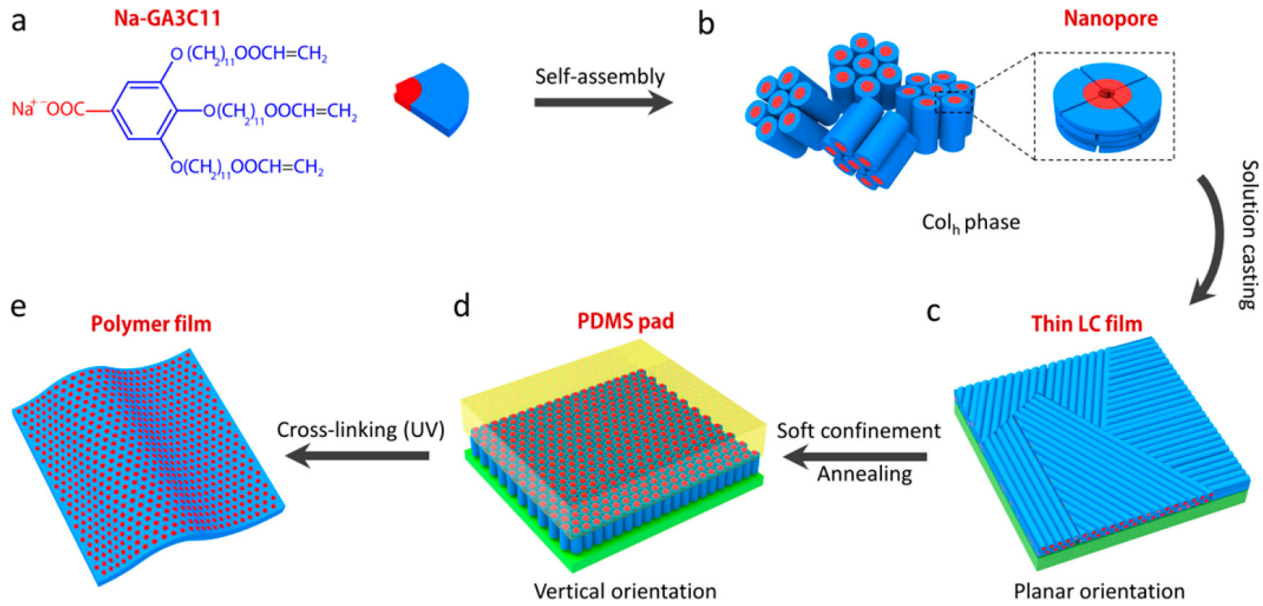


Figure 1: The wedge shaped liquid crystal monomer (a) self assembles into mesophases with hexagonally packed pores (b). The pores are made of stacked monomer disks. A sub-micron-thick film is created by casting a dilute solution of Na-GA3C11/THF solution onto a silicon substrate and allowing the solvent to evaporate. The thin film contains nanoporous columns which lie parallel to the film plane. (d) When a soft PDMS pad is imposed to the thin film, with subsequent thermal annealing, the columns align perpendicular to the film plane. (e) Photo-cross-linking of the aligned film creates a mechanically stable thin film with vertically aligned nanopores

- It will be challenging to efficiently narrow down the large design space in a laboratory setting without a robust model.
- The only source of predictive modeling for LLC systems have been macroscopic models which likely do not adequately describe transport at these length scales. may allow tuning rejection of solutes based on size?
- Choice of head group may play a role in the rejection of charged or uncharged solutes.
- Choice of counterion may influence the establishment of a Donnan potential affecting the degree to which the membrane can exclude charged species.
- A good molecular model should incorporate a detailed picture of the nanoscopic pore structure which will be crucial to understanding the role of monomer structure in membrane design.
- Molecular dynamics simulations will provide the required level of detail

Our approach to constructing a general model will follow the development of a model of a specific LLC membrane with sufficient experimental characterization.

- We have chosen to focus on assemblies formed by Na-GA3C11
- We have also narrowed our scope to the development of a model of the Col_h phase membrane.
- Compared to the H_{II} phase, the Col_h phase is a simpler starting point, due to the absence of water, and has more detailed experimental structural data.
- Despite having structural data, there is still information which experiment cannot definitively answer.

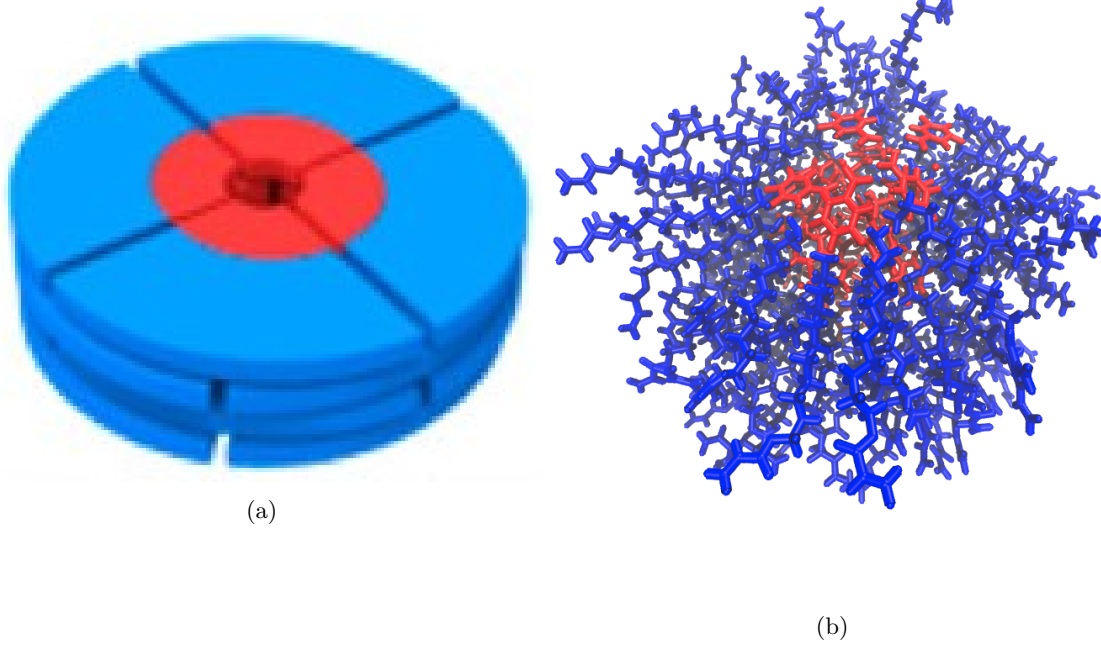


Figure 2: (a) Our previous understanding of the pore structure allows us to speculate about separation behavior. (b) A detailed molecular model will allow us to directly observe solute transport

Despite having structural data, there is still information which experiment cannot definitively answer. There are several key questions that we intend to answer which will be laid out and numbered in subsequent paragraphs.

Monomers in the Col_h system are theorized to be partitioned into stacked layers which form columnar pores. There has been no definitive answer in literature regarding the number of monomers in each layer. We want to know

1. If layers do exist, how many monomers constitute a single layer?
 - A simple molecular simulation study of a similar molecule suggested that there are 4 monomers in each layer. Their estimation is based on a simulated system containing only 16 total monomers which likely does not sufficiently model the chemical environment present in the real system. [18].
 - A separate calculation based on the volume of the liquid crystal monomers proposes that there are seven monomers in each layer [17].
 - A molecular model orders of magnitude larger than any other reported atomistic liquid crystal membrane simulations has the best chance of directly answering this question.
 - We can directly change the layer composition and note its effect on membrane structure.
2. Does our model support the existence of layers and if so, how well defined are the layers?
 - Experimentally, their existence is supported by evidence of strong π - π stacking interactions in the direction perpendicular to the membrane plane.
 - π - π stacking will only occur between the aromatic monomer head groups which leaves no description of what is happening in the monomer tail region
 - The tails may entangle isotropically while stacking order is maintained among headgroups.
3. How do monomers in each layer position themselves with respect to surrounding layers?
 - The π - π stacking interactions may be a driving force of self assembly in this system[19]
 - Gas phase ab initio studies of benzene dimers have shown a clear energetic advantage for parallel displaced and T-shaped π - π stacking conformations versus a sandwiched conformation [20].
 - Substituted benzene rings exhibit an even stronger π - π stacking attraction which favors the parallel displaced configuration in all cases except where the substitutions are extremely electron withdrawing [21, 22].
 - We can use simulated X-ray diffraction patterns to compare the two stacking configurations.
4. Is it necessary to include any water in order to appropriately model the Col_h phase?
 - While the Col_h phase is described as dry, it is possible that small amounts of ambient water may be leached into the system.
 - The hydrogen bonding network formed by the water may play a role in structuring the pore.
 - We can use simulated X-ray diffraction patterns to see if there is any meaningful structural difference between a "dry" and "wet" system

In this study, we build a significantly more realistic atomistic model of LLC membranes than has ever previously been done, and explore what new structural information can be gained and what structure hypotheses are supported by this model.

- We validate the model using as much experimental information as possible.
- We are most interested in reproducing the conclusions about structure which have been made from X-ray diffraction (XRD) experiments and in matching ionic conductivity measurements [16].
 - We have compared simulated X-ray diffraction patterns to experiment in order to match major features present in the 2D patterns.

- We calculated ionic conductivity using two agreeing methods.
- We examined the influence of crosslinking on membrane structure.
- The structure-building approach and analysis used in this paper can be readily extended to the H_{II} phase and other similar LC systems.

Methods

Liquid crystal monomers were parameterized using the Generalized AMBER Forcefield [23] with the Antechamber package [24] provided with AmberTools16 [25]. Atomic charges were assigned using tools from Openeye Scientific Software. All molecular dynamics simulations were run using the latest version of Gromacs 2016. [26, 27, 28, 29]

An ensemble of characteristic, low-energy vacuum monomer configurations were constructed by applying a simulated annealing process to a parameterized monomer.

- Monomers were cooled from 1000K to 50K over 10 nanoseconds.
- A low energy configuration was randomly pulled from the trajectory and charges were reassigned using the am1bccsym method of molcharge shipped with Openeye Scientific software's QUACPAC
- Using the new charges, the monomer system was annealed again and monomer configurations were pulled from the trajectory to be used for full system construction (Figure 3a).

The timescale for self assembly of monomers into the hexagonal phase is unknown and likely outside of a reasonable length for an atomistic simulation, calling for a more efficient way to build the system.

- Previous work has shown a coarse grain model self assemble into the H_{II} phase configuration in ≈ 1000 ns [30].
- We attempted atomistic self-assembly by packing monomers into a box using Packmol [31].
- Simulations of greater than 100 ns show no indicators of progress towards an ordered system.
- To bypass the slow self-assembly process, python scripts are used to assemble monomers into a structure close to one of a number of hypothesized equilibrium configurations (Figure 3).

A typical simulation volume contains four pores in a monoclinic unit cell, the smallest unit cell that maintains hexagonal symmetry when extended periodically.

- Each pore is made of twenty stacked monomer layers with periodic continuity in the z direction, avoiding any edge effects and creating an infinite length pore ideal for studying transport.
- A small number of layers is preferred in order to reduce computational cost and to allow us to look at longer timescales.
- Ultimately, we chose to build a system with 20 monomer layers in each pore in order to obtain sufficient resolution when simulating X-ray diffraction patterns. This point will be explained in more detail later.
- We chose initial guesses for the remaining structural parameters based on experimental data and treated them as variables during model development.

We used experimental wide angle X-ray scattering (WAXS) data (produced as described in [12]) and small angle X-ray scattering (SAXS) data from [16] to inform our choices of some initial structural parameters (Figure 4). We rely primarily on the 2D WAXS data since it encodes all structural details down to the sub-nm scale.

- There are five major features of interest present in the 2D experimental pattern shown in Figure 4b.

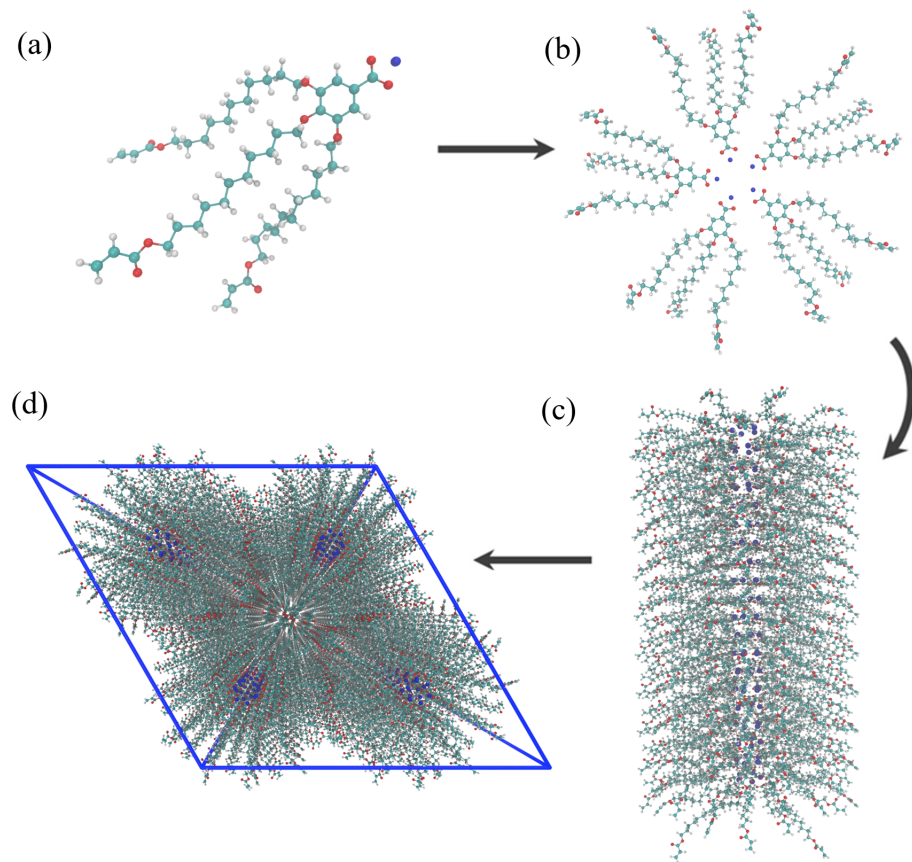


Figure 3: (a) A single monomer was parameterized and annealed to produce a low energy configuration. (b) Monomers are rotated and assembled into layers with hydrophilic centers. (c) Twenty layers are stacked on top of each other to create a pore. (d) Pores are duplicated and placed into a monoclinic unit cell

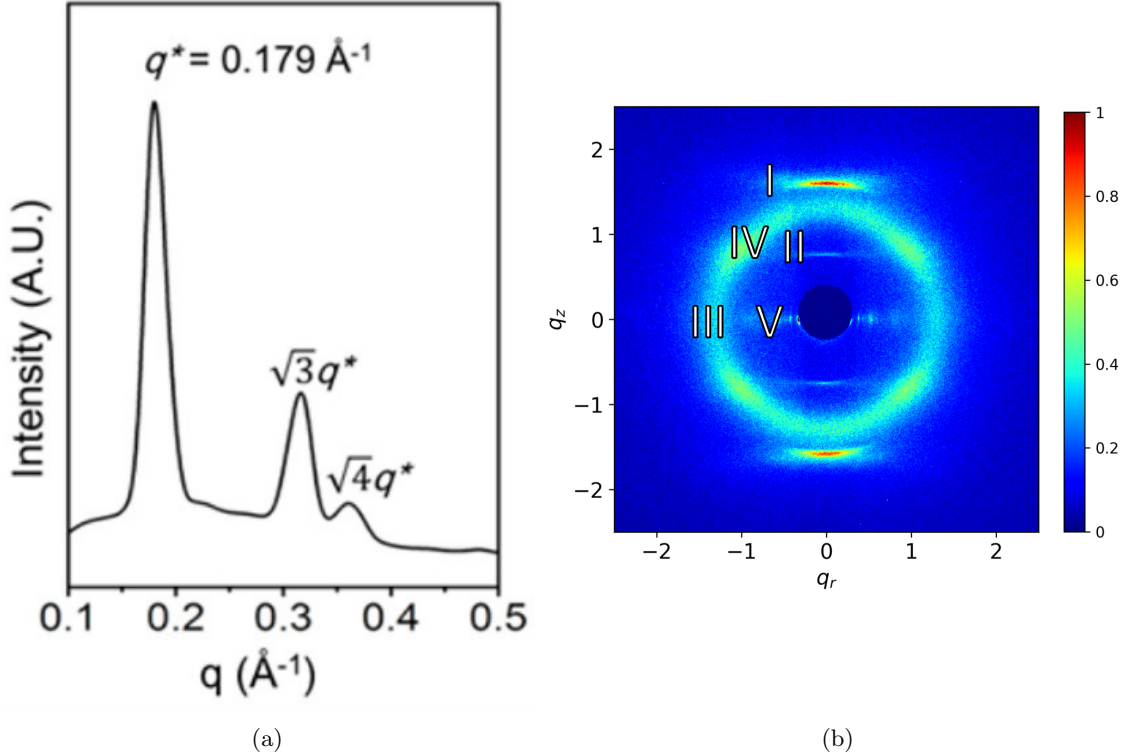


Figure 4: (a) 1D small angle X-ray scattering indicates hexagonal packing of pores as well as the spacing between pores (b) 2D wide angle X-ray scattering gives details about repeating features less than 1 nanometer apart

- The first is located at $q_z = 1.7 \text{ \AA}^{-1}$, corresponding to a real spacing of 3.7 \AA . The reflection is attributed to π - π stacking between aromatic rings in the direction perpendicular to the membrane plane, or z-axis [12]. For simplicity, this reflection will be referred to as R- π .
 - A weak intensity line is located at exactly half the q_z value of R- π ($q_z = 0.85 \text{ \AA}^{-1}$), corresponding to a real space periodic spacing of 7.4 \AA . This reflection has been interpreted as 2_1 helical ordering of aromatic rings along the z axis meaning if the positions of the aromatic rings can be traced by a helix, then for each turn in the helix, there should be two aromatic rings. For this reason it will be referred to as R-helix.
 - A third major reflection is marked by a low intensity ring located at $r = 1.4 \text{ \AA}^{-1}$. The real space separation corresponds to 4.5 \AA which is characteristic of the average spacing between packed alkane chains. This reflection will be called R-alkanes.
 - Within R-alkanes, are four spots of higher relative intensity which will be called R-spots. All are located ≈ 40 degrees from the q_z axis in their respective quadrants. In many liquid crystal systems this can be explained by the tilt angle of the alkane chains with respect to the xy plane.
 - The final feature corresponds to the spacing and symmetry of the d_{100} plane which can be related to the distance between pores. The feature, which will be called R-pores, is characterized by dots along $q_z = 0$. The spacing between dots is indicative of the hexagonal symmetry of the packed pores. The same information at higher resolution is obtained using a SAXS setup. By radially integrating the 2D data one gets a 1D curve which is shown in Figure 4a.

We chose the initial layer spacing based on $R\pi$.

- Each monomer was rotated so the plane of the aromatic head groups would be parallel to the xy plane.

- The layers are placed so aromatic rings are stacked 3.7 Å apart in the z-direction.
- To quantify the degree of layering in our system, we calculated a spatial correlation function, $g(z)$, measured along the z-axis (perpendicular to the membrane plane)
- To calculate $g(z)$, we binned the z component distances between the center of mass of each benzene ring and all others of the same pore over 50 ns of equilibrated trajectory and then normalized by the average number density.
- We compare the degree of layering between systems based on the amplitude of the first peak in $g(z)$. We halve the difference between the maximum of the first peak and the following minimum. We compare the difference to the mean to get a percentage deviation from the average number density.
- To extract the average distance between layers we applied a discrete fourier transform to $g(z)$ and extracted the highest intensity frequency

We placed pores at a chosen initial spacing based on R-pores, then allowed the system to settle into its preferred spacing.

- The model's pore centers are spaced 4.5 nm apart initially, $\approx 10\%$ larger than the experimental value of 4.12 nm in order to reduce unintended repulsions resulting from a tightly packed initial configuration.
- To calculate the equilibrated pore spacing, we measured the distance between pore centers.
- Pore centers were located by averaging the coordinates of sodium ions in their respective pores.
- Statistics were generated using the bootstrapping technique (See Supplemental Information)
 - For each bootstrap trial, we recreate an equilibrium trajectory by randomly sampling from the original trajectory
 - Each pore spacing has its own trajectory with its own average value
 - The average value of each pore spacing is averaged to get the overall average pore spacing
 - The standard deviation of average values is reported as the uncertainty in pore spacing
 - We are interested in 5 pore-to-pore distances which should all be equal in a perfect hexagonal array. Only 4 are independent

We used experimental Transmission electron microscopy (TEM) and size exclusion rejection data [12, 16, 14] to inform our definition of pore radius in the initial configuration.

- Experimental evidence suggests uniform pores with radii of 0.6 nm
- Comparing a geometric measurement of pore size derived from an atomistic model, to a less precise, experimentally derived pore size estimate, will give ambiguous results.
- What is meant by pore radius will not be clear until we establish a clear picture of the nanoscopic pore environment.
- When constructing pores, we chose the carboxylate carbon from the monomer head group as a reference atom, and placed it a distance r from the pore center, where r is the pore radius (5).
- We will not make direct comparisons of pore radius between our model and experiment to avoid the ambiguity, however, we do define a pore radius for our own purposes.

The relative interlayer orientation was chosen based on clues from diffraction data as well as the various known stacking modes of benzene and substituted benzene rings: sandwiched, parallel-displaced and T-shaped [20] (Figures 6a to 6c).

- The T-shaped configuration was ruled out based on the inconsistency of its ≈ 5 Å equilibrium stacking distance [20].

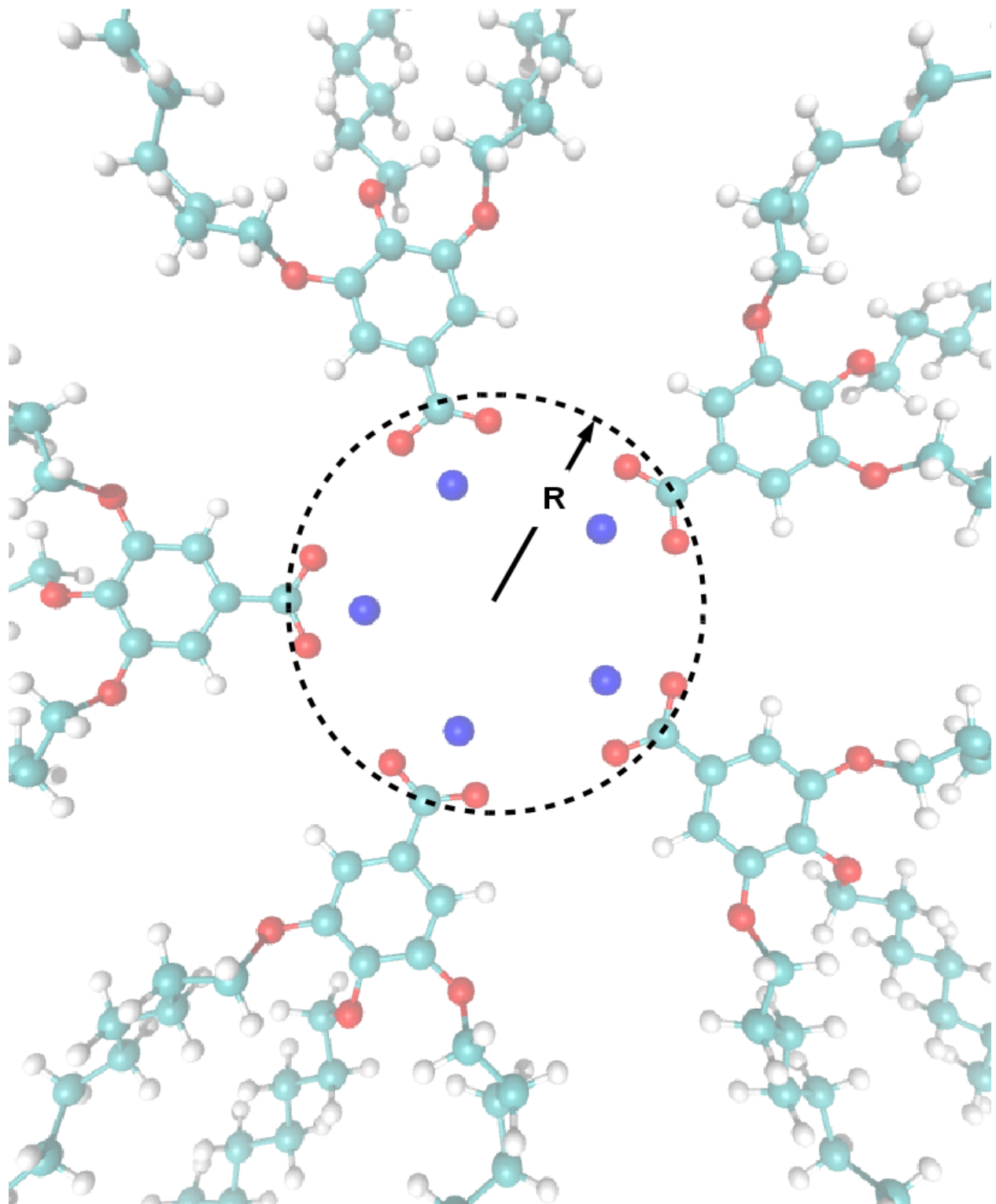


Figure 5: The pore radius of the initial configuration is defined using the carboxylate carbon as a reference

- The system's preference towards the sandwiched vs. parallel displaced stacking modes will be explored.
- Both have reported stacking distances near the $R-\pi$ value of 3.7 Å
- Headgroups in the sandwiched configuration are stacked directly on top of each other while stacked headgroups in the parallel displaced configuration are offset by $180/n_{mon}$ degrees where n_{mon} equals the number of monomers per layer.

We developed equilibration schemes to create dry and wet configurations. Both schemes start with an initial configuration generated according to the previous guidelines.

- Dry equilibration scheme:
 - Restraints fix monomer head groups in the sandwiched or parallel-displaced configurations while allowing monomer tails to settle.
 - Doing so also mitigates system dependence on initial monomer configuration.
 - The restrained portion of the equilibration scheme is run in the NVT ensemble.
 - Every 50 ps, we reduce the force constants by the square root of its previous value, starting from 1e6 KJ mol⁻¹ nm⁻².
 - Once the force constant is below 10 KJ mol⁻¹ nm⁻², the restraints are slowly released until there is no more restraining potential.
 - The resulting unrestrained structure is allowed to equilibrate for 5 ns in the NPT ensemble with pressure controlled by the berendsen barostat.
 - Long, NPT equilibration simulations are run for at least 400 ns using the Parrinello-Rahman barostat with a time constant of 10 ps.
- Wet equilibration scheme:
 - In order to create a wet system, we solvated an initial configuration with water using gmx solvate
 - All waters placed outside the pore region are removed
 - Waters inside the pore region are randomly removed until the desired concentration of water in the pores is reached.
 - The remainder of the equilibration is the same as the dry system
- In all cases, the v-rescale thermostat was used with tau-t = 0.1

Simulated X-ray diffraction patterns were generated based on atomic coordinates for a direct experimental comparison.

- All atomic coordinates were simulated as gaussian spheres of electron density corresponding to each atom's atomic number.
- A three dimensional fourier transform (FT) of the array of electron density results in a three dimensional structure factor which represents the unit cell in reciprocal space. z axis to generate a 2D cross section close to what one would see experimentally.
- We matched experimental 2D WAXS patterns by iterative improvement of our choice of initial structure and equilibration procedure.

We calculated ionic conductivity using two different methods for robustness.

- The Nernst-Einstein relation relates the DC ionic conductivity to ion diffusivity, D , concentration, C , ion charge, q , the boltzmann constant, k_b , and temperature, T :

$$\sigma = \frac{q^2 C D}{k_b T}$$

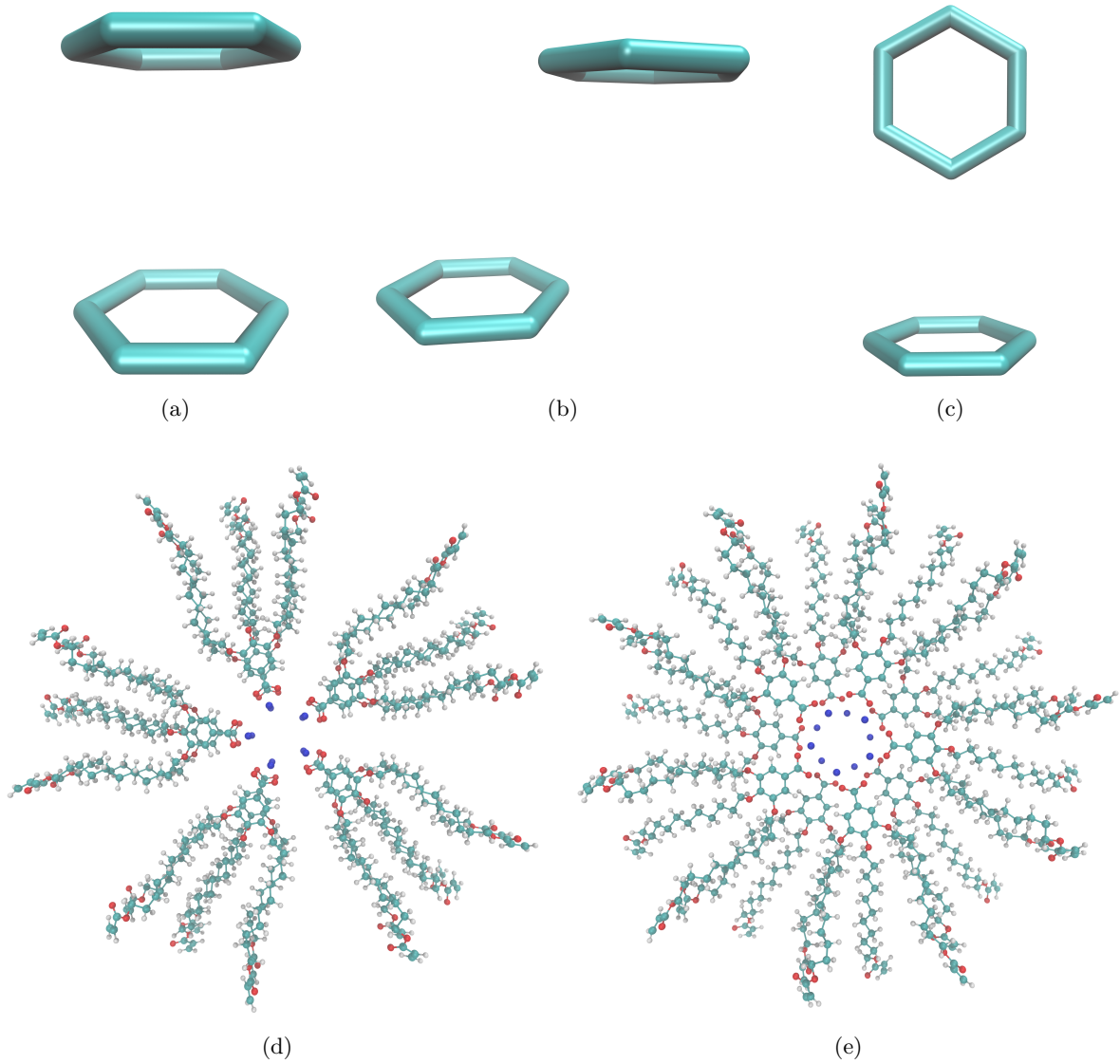


Figure 6: (a) Sandwiched benzene dimers stack 3.8 Å apart. (b) Parallel-Displaced benzene dimers stack 3.4 Å vertically and 1.6 Å horizontally apart. (c) T-shaped benzene dimers stack 5.0 Å apart. (d) Two monomer layers stacked in the sandwiched configuration (e) Two monomer layers stacked in the parallel-displaced configuration

- Sodium ion diffusion coefficients were found by calculating the slope of the linear region of the mean square displacement curve as indicated by the einstein relation [32].
- We looked at the MSD plot to determine where to begin and end a linear fit
- Ion concentration was measured with respect to the entire unit cell.
- The second method, termed the 'Collective Diffusion' model, measures the movement of the collective variable, Q, which is defined as the amount of charge transfer through the system and can be thought to represent the center of charge of the system.
- The conductance, γ of the system can be calculated as:

$$\gamma = \frac{D_Q}{k_b T}$$

Conversion to ionic conductivity is achieved by multiplying by channel length and dividing by the membrane cross sectional area.

- D_Q is the diffusion coefficient of the collective variable Q. It can be calculated using the einstein relation.
- A full derivation of the model can be accessed elsewhere [33].

Using an equilibrated structure, a crosslinking procedure was performed in order to match synthetic procedures.

- The purpose of crosslinking is to maintain macroscopic alignment of the crystalline domains, ensuring aligned, hexagonally packed pores.
- For that reason, we are not concerned with replicating the kinetics of the reaction, but instead emphasize the consistency of the final structure with experimental structural data.
- The algorithm was developed based on the known reaction mechanism.
- Crosslinking of this system is a free radical polymerization (FRP) taking place between terminal vinyl groups present on each of the three monomer tails.
- FRPs require an initiator which bonds to the system, meaning new atoms were introduced into the system.
- For simplicity, the initiator was simulated as hydrogen and made present in the simulation by including them in all possible bonding positions as dummy atoms.
- The crosslinking procedure is carried out iteratively.
- During each iteration, bonding carbon atoms are chosen based on a distance cut-off.
- The topology is updated with new bonds and dummy hydrogen atoms are changed to appropriate hydrogen types.
- Head-to-tail addition was the only propagation mode considered due to its dominance in the real system.
- Direction of attack was not considered because the resultant mixture is racemic.

Results and Discussion

Determination of Nanoscopic Structural Details

We will now address the questions raised in the introduction in the order that they were asked.

To discern the composition of the monomer layers, addressing (1), we ran simulations of systems created with 4 - 8 monomers per layer.

- We created systems in both the parallel displaced and sandwiched configurations
- All systems were prepared according to the dry equilibration procedure
- All systems are stable after 400 ns of simulation.
- Table 8 shows the pore spacing for all systems tested.
- Systems built with 5 monomers in each layer equilibrate to a pore spacing that is most consistent with the experimental value of 4.12 nm derived from SAXS measurements (Figure 4a).
- The remainder of this discussion will focus on the analysis of systems built with 5 monomers per layer.

To answer (2), we verified that the system stays partitioned into layers by plotting the pair correlation function, $g(z)$ calculated between atoms along the length of the pores (Fig 7).

- We measured $g(z)$ with respect to aromatic rings in the head groups and, separately, with respect to carbon atoms on the alkane chains.
- In both cases, we see a degree of layer partitioning
- Using the head groups as reference, we see that sandwiched configuration layers stack 4.29 Å apart while parallel displaced configuration layers stack 4.37 Å apart.
- Using the alkane chain carbons as reference we see a layer spacing of 4.39 Å and 4.38 Å in the sandwiched and parallel displaced configurations respectively.
- The power spectrums used to calculate the reported layer spacings are given in the Supplemental Information.
- We see a difference in the spacing in the head group versus tail region because there is more volume to fill with less densely packed carbon chains in the tail region.
- Even though the layer spacing is similar, the sandwiched configuration exhibits more defined layers with its first peak deviating from the mean number density by 61 %.
- The parallel displaced configuration deviates from the mean by only 12 % in comparison.

We answer question (3) by simulating X-ray diffraction patterns produced from equilibrated MD trajectories.

- Systems of 5 monomers per layer in the parallel displaced and sandwiched configurations were tested.
- Simulated patterns were generated using portions of simulation trajectory after equilibration.
- The patterns for both structures are shown and compared to experiment in Figure ??.

Simulated XRD of the sandwiched configuration contains all experimental features except for R-helix.

- R-alkanes and R-pores appear in the expected locations.
- R- π is also present, intersecting R-alkanes at a lower q value than in experiment. The rings prefer to stack $\approx 4.2\text{\AA}$ apart as opposed to 3.7\AA .

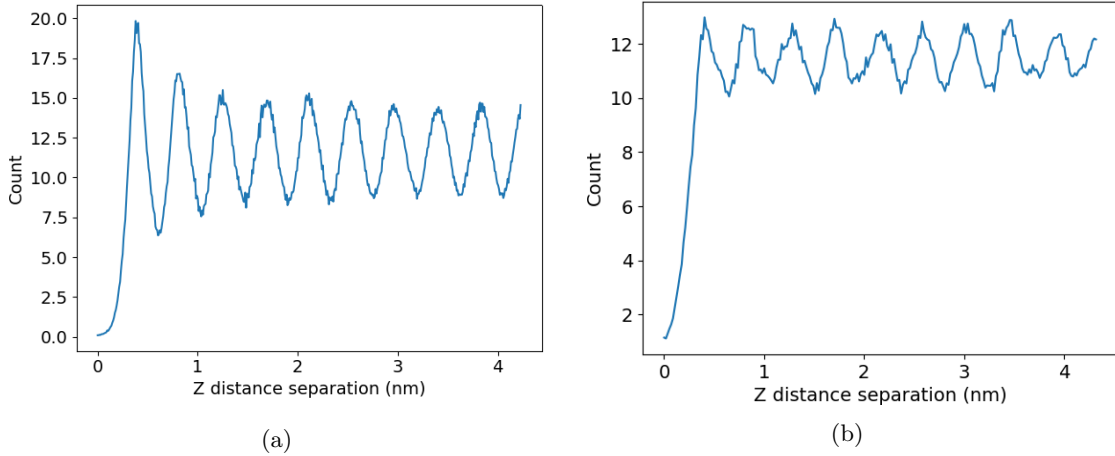


Figure 7: Pair distribution functions of aromatic carbons for the (a) 5 monomer per layer, sandwiched and (b) 5 monomer per layer, parallel displaced configurations. Clear periodic maxima in the z probability density indicate distinct layers. The magnitude of the spikes with respect to the average suggest that the 5 monomer per layer, sandwiched configuration possesses a higher degree of layer partitioning.

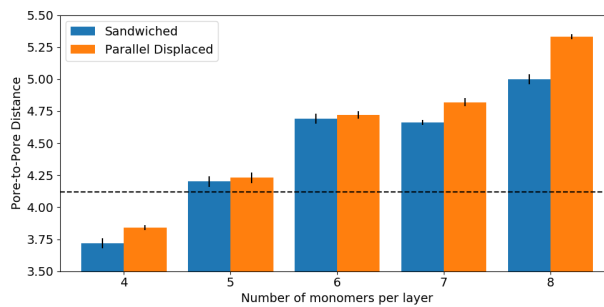


Figure 8: The pore spacing (given in nm) of the model increases as number of monomers in each layer increases. The pore spacing of a system starting in the sandwiched configuration is systematically lower than that started in an offset configuration. Systems built with 5 monomers per layer in a parallel displaced configuration result in a pore spacing closest to the experimental 4.12 nm

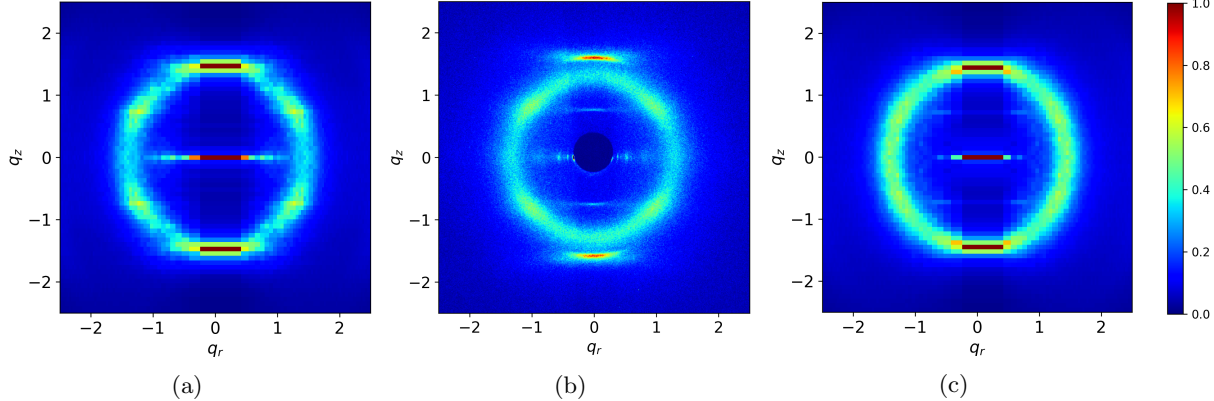


Figure 9: The simulated X-ray diffraction patterns for simulations run in the sandwiched (a) and parallel-displaced (c) configurations are compared to experiment (b). The parallel displaced configuration is the only one that exhibits all major reflections of interest to some degree

- Most notably, R-spots appears in the expected location, which suggests that there is something intrinsic to closer packing that gives rise to such features.

The parallel displaced configuration results in a simulated XRD pattern with the closest match to experiment.

- It produces the only pattern that exhibits all major reflections
- R-alkanes, R-pores and R- π appear as they do in the sandwiched configuration.
- R-spots appears, however with a lower intensity relative to R-alkanes when compared to the sandwiched configuration.
- R-helix appears apparently due to the parallel displaced aromatic rings

R-spots, which appears in both simulated XRD patterns, is a result of the way alkane tails pack together.

- Previously, the spots in the diffraction pattern had been explained as the product of tilted alkane chains.
- We measured the tilt angle of the alkane chains and showed that our system equilibrates to an average tilt angle close to zero degrees 10
- To understand the origin of the spots, we determined which atoms gave rise to the feature
- Since R-spots is present as higher intensity spots within R-alkanes, it is likely that the spots arise as a consequence of the tails.
- By removing atoms from the trajectory and simulating a diffraction pattern, we were able to isolate the cause of the spots to the tails (Figure 11).
- Since the tails stay nearly flat, we plotted the centroids of the tails and measured the angle between each centroid and its nearest neighbors with respect to the plane of the membrane (Figure ??).
- We see distinct peaks in the distribution of these angles (Figure 12)

The peaks in the tilt angle distribution are consistent with the location of R-spots.

- The peaks of interest in Figures 12a and ?? are located at $\pm 33^\circ$ which is the same location where the highest intensity of spots are located on the simulated patterns

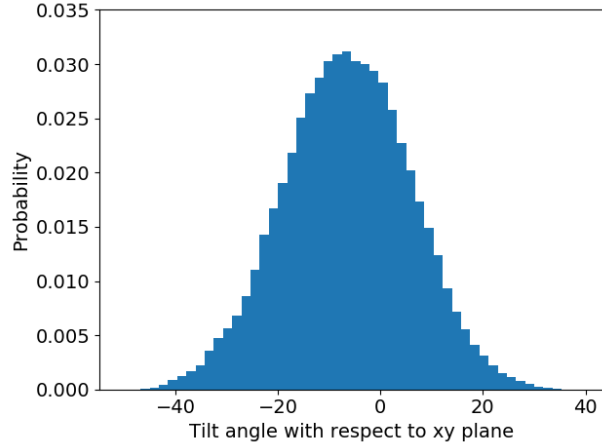


Figure 10: The tilt angle distribution of alkane chain tails with respect to the membrane plane indicates an average tilt angle near 7° which is far from the 37° tilt angle previously used to explain R-spots

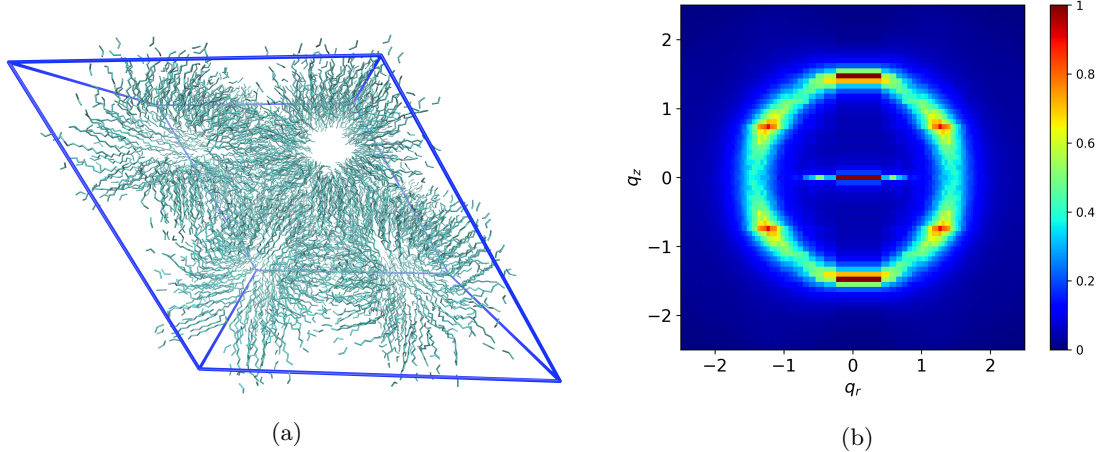


Figure 11: (a) All atoms except carbon atoms making up the tails are removed from the trajectory. (b) The simulated diffraction pattern of the tail-only trajectory still shows R-spots

- We confirmed this conclusion by radially integrating the 2D WAXS pattern for q values between 1.57 and 1.4 (real space between 4 and 4.5 Å)
- We observe that distinct peaks appear c.a. 30° , in close agreement with the previously measured angle distribution (12b 12d)
- We performed the same integration on the raw experimental data and found the angle at which R-spots reaches its highest intensity to be $\pm 37^\circ$ which is a reconcilable difference with our simulated results.

We answer (4) and further support (3) by preparing parallel displaced and sandwiched configurations according to the wet equilibration procedure.

- We do not have an experimental measurement of water in the pores
- We tested a range of water concentrations from 0.5 to 5 percent
- Our lower bound represents a system with on average 2 water molecules for each monomer layer.
- Figure ?? shows results for each configuration.

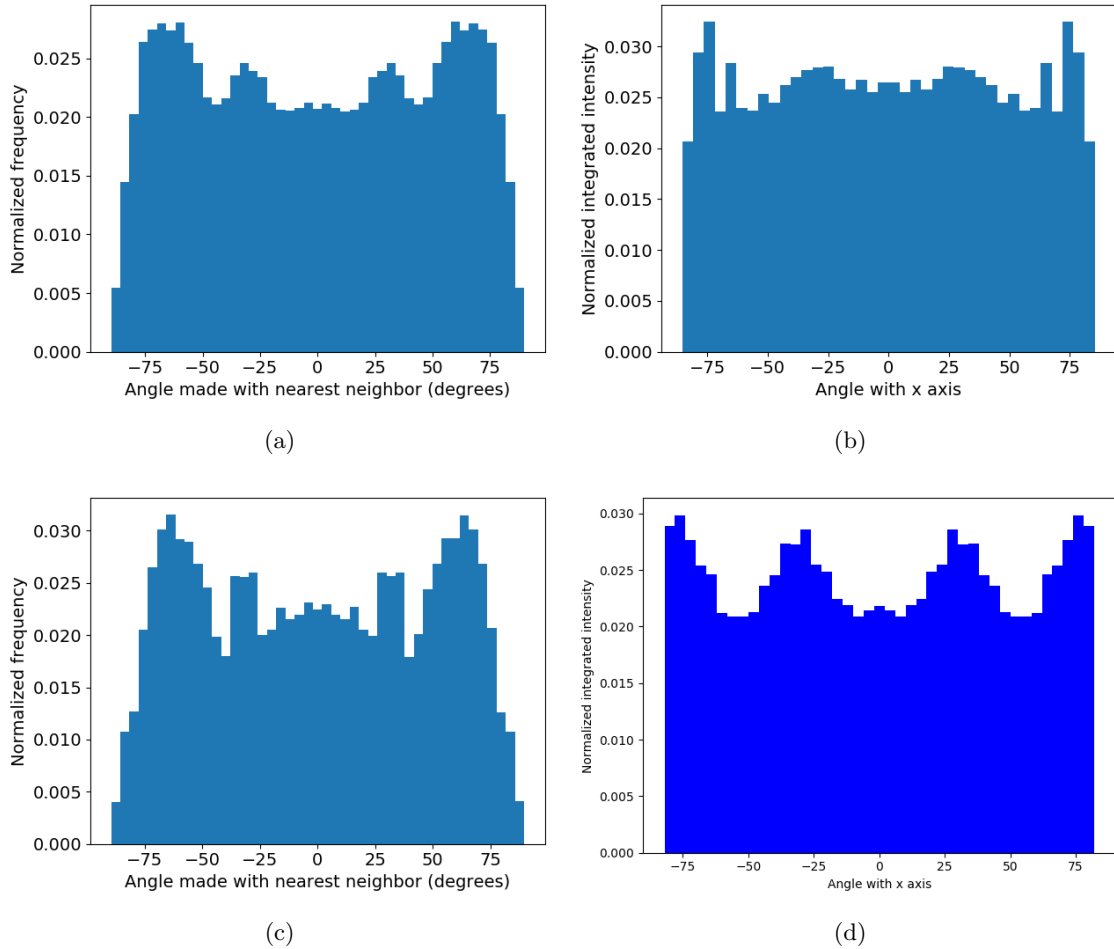


Figure 12: The distribution of angles w.r.t. the xy plane between alkane chain tail centroids and nearest neighbor centroids for equilibrated parallel displaced (a) and sandwiched (c) configurations. The same peaks are visible when the 2D simulated diffraction data is radially integrated in the R-alkanes region, (b) and (d) respectively.

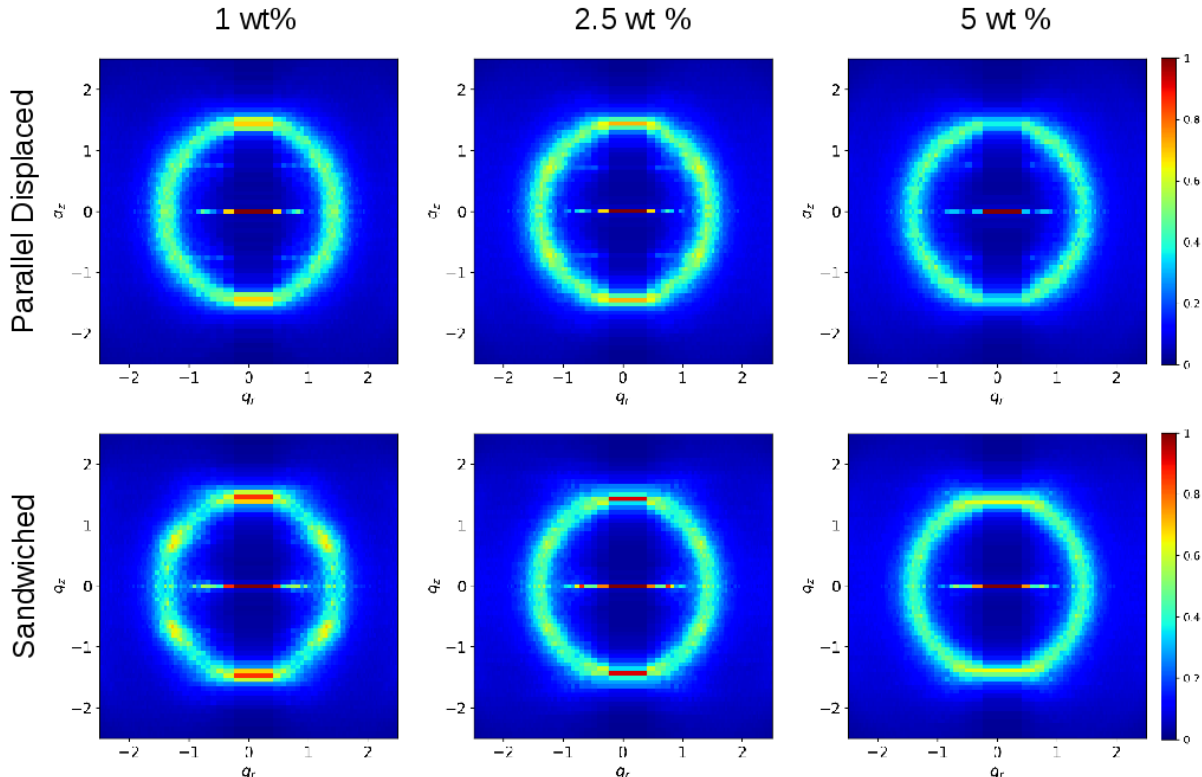


Figure 1: Simulated diffraction patterns generated from trajectories of systems built in the parallel displaced and sandwiched configurations as a function of water content shows weaker reflections than the dry system. All plots are scaled to use the same colorbar as their dry system counterpart

In all cases, water disrupts structuring of the model.

- The plots in Figure ?? are normalized to have the same colorbar as the dry systems.
- The intensity of the reflections decrease when water is added to the system.
- In systems built with 5 weight percent water, R- π and R-spots become nearly indistinguishable from R-alkanes.

Water is not needed to obtain and simulate the correct equilibrium membrane structure.

- We note that water absorbed during membrane synthesis may be present in far lower concentrations than those tested here.
- We do not eliminate the possibility that water is necessary in order to drive self-assembly. Studying the mechanisms of self assembly is beyond the scope of this work.
- However, once the system has formed the Col_h phase, adding water only drives disorder in the structure
- In the equilibrium configuration, if water exists, it is confined to the pore region where there is no driving force for aggregation of water molecules.
- In the case of trace water, water molecules will be too sparse to form a hydrogen bonding network.

Ionic conductivity calculation

We use the equilibrated parallel displaced system to calculate ionic conductivity since its structure is the closest match to experiment. The model gives reasonable estimates of ionic conductivity when compared to experiment.

- Calculated values of ionic conductivity obtained using the Nernst Einstein relation and Collective Diffusion model are compared in Figure 14.
- The two methods agree with each other within error, although the uncertainty obtained using the Collective Diffusion model is much higher.
- Much longer simulations are needed to lower the uncertainty, however it is not feasible to do so with a large model.
- For this reason we will likely only use the Nernst Einstein relation in future calculations of this type.

The calculated values of ionic conductivity are higher than experiment by an order of magnitude.

- One can justify the reason for this result by considering the real system studied experimentally
- The ionic conductivity measurement to which we are comparing was done on a 80 μm thick film, nearly 10,000 times thicker than our simulated system.
- The thick film likely has defects leading to non-contiguous pores and imperfect alignment.
- The 2D SAXS pattern shows the small degree of tortuosity present in the system (13)
- It has been shown that there is a large dependence of Ionic conductivity on the alignment of the pores
- The ionic conductivity of an unaligned film is 85 times lower than that of a nearly aligned film referenced here
- It is not unreasonable that a thin, perfectly aligned film would have a value of ionic conductivity in agreement with our model

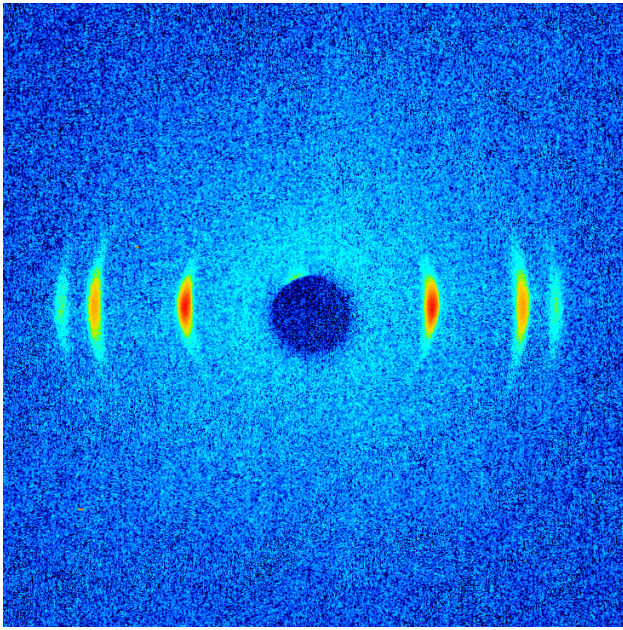


Figure 13: The experimental two dimensional SAXS pattern exhibits reflections resulting from highly aligned pore regions. A perfectly aligned system would exhibit sharp dots at the same locations of the refelctions shown. An isotropically aligned system the reflections would appear as rings centered about the origin

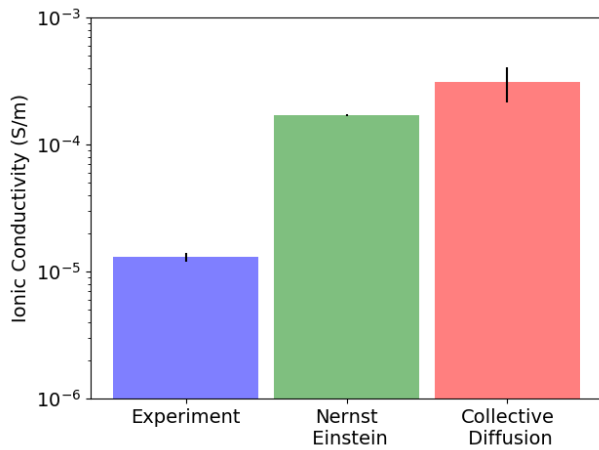


Figure 14: Calculated ionic conductivity using the Nernst-Einstein relation and Collective Diffusion model agree with error. Both methods give calculated values of ionic conductivity an order of magnitude higher than the experimental value

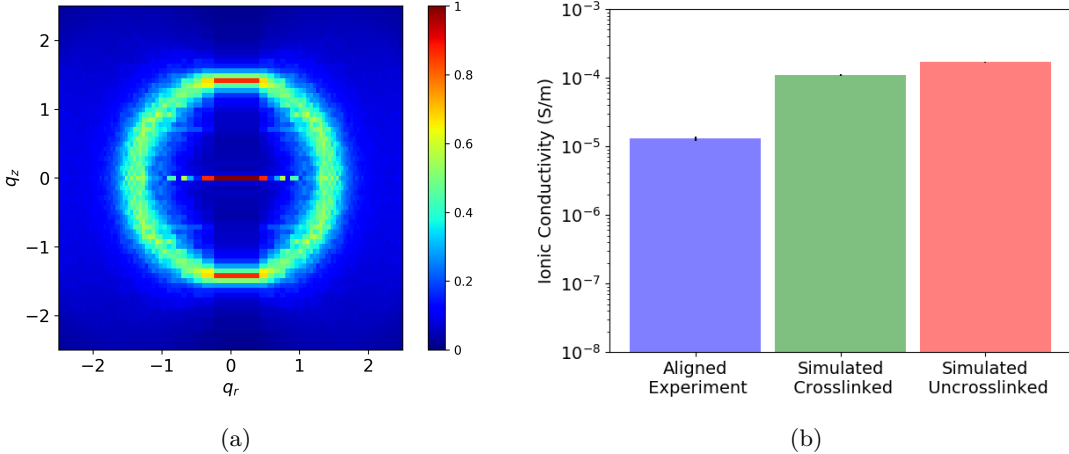


Figure 15: (a) Reflections produced by the crosslinked configuration fade relative to the uncrosslinked system. The colorbar shown is the same used for the uncrosslinked system. (b) The ionic conductivity is smaller relative to the uncrosslinked system, but still much larger than the experimental value

Implementation of the crosslinking algorithm

We applied the crosslinking algorithm to the equilibrated parallel-displaced configuration with 5 monomers per layer.

- We reach 95 % conversion of terminal vinyl groups
- The distance between pores shrinks by 0.4 Å after the system is crosslinked
- We simulated the crosslinked system in the NPT ensemble for 100 ns
- Major features are still present in the X-ray diffraction, however at lower intensities 15a
- The ionic conductivity is lower in the crosslinked system 15b

Conclusion

We have used a detailed molecular model of the Col_h phase formed by NA-GA3C11 in order to study the nanoscopic structure.

- While there have been efforts to model formation of various liquid crystalline phases with molecular dynamics, to our knowledge there have been no studies which attempt to examine their structure with the same level of detail presented here.
- We were able to deduce that layers are composed of 5 monomers
- We have confirmed that monomers stay partitioned in layers.
- We have explored the affect of two different π - π stacking modes on the equilibrated membrane strucure.
- Simulated diffraction patterns generated from MD trajectories suggest that the parallel-displaced configuration produces a structure with the closest match to experiment.
- Finally, water is not needed to maintain membrane structure
- Now that we have a good idea of what the membrane structure should look like, we will evaluate transport of various solutes within the system.

- We will apply the knowledge gained from this study in order to suggest improvements to the existing system as well as to evaluate new unsynthesized LLC systems.

References

- [1] T. Humplik, J. Lee, S. C. OHern, B. A. Fellman, M. A. Baig, S. F. Hassan, M. A. Atieh, F. Rahman, T. Laoui, R. Karnik, and E. N. Wang, "Nanostructured materials for water desalination," *Nanotechnology*, vol. 22, no. 29, p. 292001, 2011.
- [2] B. Van Der Bruggen, C. Vandecasteele, T. Van Gestel, W. Doyen, and R. Leysen, "A review of pressure-driven membrane processes in wastewater treatment and drinking water production," *Environmental Progress*, vol. 22, pp. 46–56, Apr. 2003.
- [3] X. Song, Z. Liu, and D. D. Sun, "Nano Gives the Answer: Breaking the Bottleneck of Internal Concentration Polarization with a Nanofiber Composite Forward Osmosis Membrane for a High Water Production Rate," *Advanced Materials*, vol. 23, pp. 3256–3260, Aug. 2011.
- [4] R. L. McGinnis and M. Elimelech, "Global Challenges in Energy and Water Supply: The Promise of Engineered Osmosis," *Environmental Science & Technology*, vol. 42, pp. 8625–8629, Dec. 2008.
- [5] J. G. Wijmans and R. W. Baker, "The solution-diffusion model: a review," *Journal of Membrane Science*, vol. 107, pp. 1–21, Nov. 1995.
- [6] W. R. Bowen and J. S. Welfoot, "Modelling the performance of membrane nanofiltrationcritical assessment and model development," *Chemical Engineering Science*, vol. 57, pp. 1121–1137, Apr. 2002.
- [7] D. Cohen-Tanugi, L.-C. Lin, and J. Grossman, "Multilayer Nanoporous Graphene Membranes for Water Desalination," *Nano Letters*, vol. 16, pp. 1027–1033, Jan. 2016.
- [8] K. Hata, D. N. Futaba, K. Mizuno, T. Namai, M. Yumura, and S. Iijima, "Water-Assisted Highly Efficient Synthesis of Impurity-Free Single-Walled Carbon Nanotubes," *Science*, vol. 306, pp. 1362–1364, Nov. 2004.
- [9] S. Maruyama, E. Einarsson, Y. Murakami, and T. Edamura, "Growth process of vertically aligned single-walled carbon nanotubes," *Chemical Physics Letters*, vol. 403, pp. 320–323, Feb. 2005.
- [10] S. MURAD, K. ODER, and J. LIN, "Molecular simulation of osmosis, reverse osmosis, and electroosmosis in aqueous and methanolic electrolyte solutions," *Molecular Physics*, vol. 95, pp. 401–408, Oct. 1998.
- [11] L. Li, J. Dong, T. M. Nenoff, and R. Lee, "Desalination by reverse osmosis using MFI zeolite membranes," *Journal of Membrane Science*, vol. 243, pp. 401–404, Nov. 2004.
- [12] X. Feng, M. E. Tousley, M. G. Cowan, B. R. Wiesnauer, S. Nejati, Y. Choo, R. D. Noble, M. Elimelech, D. L. Gin, and C. O. Osuji, "Scalable Fabrication of Polymer Membranes with Vertically Aligned 1 nm Pores by Magnetic Field Directed Self-Assembly," *ACS Nano*, vol. 8, pp. 11977–11986, Dec. 2014.
- [13] R. C. Smith, W. M. Fischer, and D. L. Gin, "Ordered Poly(p-phenylenevinylene) Matrix Nanocomposites via Lyotropic Liquid-Crystalline Monomers," *Journal of the American Chemical Society*, vol. 119, no. 17, pp. 4092–4093, 1997.
- [14] M. Zhou, T. J. Kidd, R. D. Noble, and D. L. Gin, "Supported Lyotropic Liquid-Crystal Polymer Membranes: Promising Materials for Molecular-Size-Selective Aqueous Nanofiltration," *Advanced Materials*, vol. 17, pp. 1850–1853, Aug. 2005.
- [15] R. Resel, U. Theissl, C. Gadermaier, E. Zojer, M. Kriechbaum, H. Amenitsch, D. Gin, R. Smith, and G. Leising, "The H2-phase of the lyotropic liquid crystal sodium 3,4,5-tris(omega-acryloyloxyundecyloxy)benzoate," *Liquid Crystals*, vol. 27, pp. 407–411, Mar. 2000.
- [16] X. Feng, S. Nejati, M. G. Cowan, M. E. Tousley, B. R. Wiesnauer, R. D. Noble, M. Elimelech, D. L. Gin, and C. O. Osuji, "Thin Polymer Films with Continuous Vertically Aligned 1 nm Pores Fabricated by Soft Confinement," *ACS Nano*, vol. 10, pp. 150–158, Jan. 2016.

- [17] R. Resel, G. Leising, P. Markart, M. Kriechbaum, R. Smith, and D. Gin, “Structural properties of polymerised lyotropic liquid crystals phases of 3,4,5-tris(\$mega\$-acryloxyalkoxy)benzoate salts,” *Macromolecular Chemistry and Physics*, vol. 201, no. 11, pp. 1128–1133, 2000.
- [18] X. Zhu, M. Scherbina, A. Bakirov, B. Gorzolnik, S. Chvalun, U. Beginn, and M. Moller, “Methacrylated Self-Organizing 2,3,4-Tris(alkoxy)benzenesulfonate: A New Concept Toward Ion-Selective Membranes,” *ACS: Chemistry of Materials*, vol. 18, no. 19, pp. 4667–4673, 2006.
- [19] E. Gazit, “A possible role for -stacking in the self-assembly of amyloid fibrils,” *The FASEB Journal*, vol. 16, pp. 77–83, Jan. 2002.
- [20] M. O. Sinnokrot, E. F. Valeev, and C. D. Sherrill, “Estimates of the Ab Initio Limit for Interactions: The Benzene Dimer,” *Journal of the American Chemical Society*, vol. 124, pp. 10887–10893, Sept. 2002.
- [21] M. P. Waller, A. Robertazzi, J. A. Platts, D. E. Hibbs, and P. A. Williams, “Hybrid density functional theory for -stacking interactions: Application to benzenes, pyridines, and DNA bases,” *Journal of Computational Chemistry*, vol. 27, pp. 491–504, Mar. 2006.
- [22] A. L. Ringer, M. O. Sinnokrot, R. P. Lively, and C. D. Sherrill, “The Effect of Multiple Substituents on Sandwich and T-Shaped Interactions,” *Chemistry A European Journal*, vol. 12, pp. 3821–3828, May 2006.
- [23] J. Wang, R. M. Wolf, J. W. Caldwell, P. A. Kollman, and D. A. Case, “Development and testing of a general amber force field,” *Journal of Computational Chemistry*, vol. 25, pp. 1157–1174, July 2004.
- [24] J. Wang, W. Wang, P. A. Kollman, and D. A. Case, “Automatic atom type and bond type perception in molecular mechanical calculations,” *Journal of Molecular Graphics and Modelling*, vol. 25, pp. 247–260, Oct. 2006.
- [25] D. Case, R. Betz, W. Botello-Smith, D. Cerutti, T. Cheatham, III, T. Darden, R. Duke, T. Giese, H. Gohlke, A. Goetz, N. Homeyer, S. Izadi, P. Janowski, J. Kaus, A. Kovalenko, T. Lee, S. LeGrand, P. Li, C. Lin, T. Luchko, R. Luo, B. Madej, D. Mermelstein, K. Merz, G. Monard, H. Nguyen, H. Nguyen, I. Omelyan, A. Onufriev, D. Roe, A. Roitberg, C. Sagui, C. Simmerling, J. Swails, R. Walker, J. Wang, R. Wolf, X. Wu, L. Xiao, D. York, and P. Kollman, “AmberTools16,” Apr. 2016.
- [26] H. Bekker, H. J. C. Berendsen, E. J. Dijkstra, S. Achterop, R. van Drunen, D. van der Spoel, A. Si-jbers, H. Keegstra, B. Reitsma, and M. K. R. Renardus, “Gromacs: A parallel computer for molecular dynamics simulations,” *Physics Computing*, 1993.
- [27] H. J. C. Berendsen, D. van der Spoel, and R. van Drunen, “GROMACS: A message-passing parallel molecular dynamics implementation,” *Computer Physics Communications*, vol. 91, pp. 43–56, Sept. 1995.
- [28] D. Van Der Spoel, E. Lindahl, B. Hess, G. Groenhof, A. E. Mark, and H. J. C. Berendsen, “GROMACS: Fast, flexible, and free,” *Journal of Computational Chemistry*, vol. 26, pp. 1701–1718, Dec. 2005.
- [29] B. Hess, C. Kutzner, D. van der Spoel, and E. Lindahl, “GROMACS 4: Algorithms for Highly Efficient, Load-Balanced, and Scalable Molecular Simulation,” *Journal of Chemical Theory and Computation*, vol. 4, pp. 435–447, Mar. 2008.
- [30] J. Mondal, M. Mahanthappa, and A. Yethiraj, “Self-Assembly of Gemini Surfactants: A Computer Simulation Study,” *The Journal of Physical Chemistry B*, vol. 117, pp. 4254–4262, Apr. 2013.
- [31] L. Martnez, R. Andrade, E. G. Birgin, and J. M. Martnez, “PACKMOL: A package for building initial configurations for molecular dynamics simulations,” *Journal of Computational Chemistry*, vol. 30, pp. 2157–2164, Oct. 2009.
- [32] A. Einstein, “Investigations on the theory of the brownian movement,” *Dover Publications*, 1956.
- [33] Y. Liu and F. Zhu, “Collective diffusion model for ion conduction through microscopic channels,” *Biophysical Journal*, vol. 104, pp. 368–376, Jan. 2013.